Chemical Engineering Journal 291 (2016) 298–305

Contents lists available at ScienceDirect

Chemical Engineering Journal

journal homepage: www.elsevier.com/locate/cej

A shrinking core model for steam hydration of CaO-based sorbents cycled for CO_2 capture

John Blamey [a], Ming Zhao [b], Vasilije Manovic [c], Edward J. Anthony [c], Denis R. Dugwell [a], Paul S. Fennell [a,*]

[a] Department of Chemical Engineering, Imperial College London, South Kensington, London SW7 2AZ, United Kingdom
[b] School of Environment, Tsinghua University, Beijing 100084, China
[c] Cranfield University, Cranfield, Bedfordshire MK43 0AL, United Kingdom

HIGHLIGHTS

- Steam hydration of CaO-based sorbents for CO_2 capture investigated.
- Wide range of cycling histories and hydration temperatures investigated.
- Shrinking core model for the reaction of steam with CaO developed.
- Model showed good agreement with experimental data.

ARTICLE INFO

Article history:
Received 9 March 2015
Received in revised form 24 January 2016
Accepted 25 January 2016
Available online 1 February 2016

Keywords:
Reaction engineering
Kinetics
Energy
Adsorption
CO_2 capture
Calcium looping

ABSTRACT

Calcium looping is a developing CO_2 capture technology. It is based on the reversible carbonation of CaO sorbent, which becomes less reactive upon cycling. One method of increasing the reactivity of unreactive sorbent is by hydration in the calcined (CaO) form. Here, sorbent has been subjected to repeated cycles of carbonation and calcination within a small fluidised bed reactor. Cycle numbers of 0 (i.e., one calcination), 2, 6 and 13 have been studied to generate sorbents that have been deactivated to different extents. Subsequently, the sorbent generated was subjected to steam hydration tests within a thermogravimetric analyser, using hydration temperatures of 473, 573 and 673 K. Sorbents that had been cycled less prior to hydration hydrated rapidly. However, the more cycled sorbents exhibited behaviour where the hydration conversion tended towards an asymptotic value, which is likely to be associated with pore blockage. This asymptotic value tended to be lower at higher hydration temperatures; however, the maximum rate of hydration was found to increase with increasing hydration temperature. A shrinking core model has been developed and applied to the data. It fits data from experiments that did not exhibit extensive pore blockage well, but fits data from experiments that exhibited pore blockage less well.

1. Introduction

Calcium looping is a CO_2 capture technology that has been proposed for both pre- and post-combustion capture. Its advantages include the ability to reclaim high-grade heat, the use of a relatively inexpensive, abundant and benign limestone-derived sorbent, and the potential to de-carbonise both power generation and cement manufacture. Post-combustion capture using calcium looping is currently being developed on a 1–2 MW_{th} pilot scale [1,2], with long duration trials on a smaller 200–300 kW_{th} pilot scale [3,4]. Calcium looping makes use of the reversible carbonation of CaO (see Rn. (1)) to remove CO_2 from a gas stream with a relatively low mole fraction of CO_2 and provides a gas stream of concentrated CO_2 suitable for compression and subsequent storage, in a cyclical process [5]. One aspect of the cycle that is disadvantageous is the rapid deactivation of CaO. Deactivation occurs primarily through CaO and reactive sintering – reduction of surface area and porosity associated with the high temperatures in the calcination environment and rearrangement upon reaction to form $CaCO_3$ and reform CaO. However, other mechanisms such as sulfation, ash fouling and mass loss from the system also contribute to reductions in sorbent performance. Several techniques have been proposed for enhancement of sorbent, such as periodic reactivation of spent (unreactive) sorbent by hydration, generation of synthetic sorbents, and simple doping or thermal pre-activation of natural sorbents [6,7]. The focus here is on periodic reactivation by hydration.

* Corresponding author. Tel.: +44 (0) 20 7594 6637; fax: +44 (0) 20 7594 5638.
E-mail address: p.fennell@imperial.ac.uk (P.S. Fennell).

http://dx.doi.org/10.1016/j.cej.2016.01.086
1385-8947/

Nomenclature

C	molar concentration, mol/m^3
D_e	effective diffusivity within pores, m^2/s
D_g	gas-phase diffusivity, m^2/s
D_K	Knudsen diffusivity, m^2/s
d_p	particle diameter, m
d_{pore}	pore diameter, m
k_A	first order rate constant for the reaction of CaO with steam, m/s
k_B	Boltzmann constant, J/K
k_g	mass transfer coefficient, m/s
M	molar mass, g/mol
N	number of cycles
n	number of moles, mol
p	pressure, Pa
R	universal gas constant, J/mol/K
r	radius, m
S_V	specific, BET, surface area, expressed in m^2/m^3, m^2/m^3
T	temperature, K
t	time, s
U	fluid velocity, m/s
U_{mf}	minimum fluidisation velocity, m/s
W	molar flux, mol/m^2/s
X	mole fraction
$X_{Ca(OH)_2}$	conversion to $Ca(OH)_2$
ΔH_r^θ	enthalpy of reaction under standard conditions, kJ/mol
ε_x	porosity of species x
λ	mean free path, m
μ_g	fluid viscosity, kg/m/s
ρ_g	gas density, kg/m^3
ρ_x	density of species x, kg/m^3
σ	collision diameter, m
τ_{pore}	pore tortuosity
Ω	collision integral

Subscripts for C, r, X

c/C	at the core of the particle – $CaO/Ca(OH)_2$ interface
s/S	at the surface of particles
B	in the bulk phase (not applicable to r)
E	at equilibrium (not applicable to r)

$$CaO_{(s)} + CO_{2(g)} \rightleftharpoons CaCO_{3(s)} \qquad \Delta H_r^\theta = -178\ \text{kJ/mol} \qquad \text{(Rn.1)}$$

$$CaO_{(s)} + H_2O_{(g)} \rightleftharpoons Ca(OH)_{2(s)} \qquad \Delta H_r^\theta = -109\ \text{kJ/mol} \qquad \text{(Rn.2)}$$

A simplified typical proposed calcium looping process for post-combustion CO_2 capture with a hydration step is shown in Fig. 1. Hydration of calcium oxide is not thermodynamically favoured in either the carbonator or calciner and must be performed in a separate vessel. It is desirable for the hydrator to operate at as high a temperature as possible in order to reclaim heat from the hydrator at as high grade as possible. This is especially important given that the endothermic dehydration reaction (reverse of Rn. (2)) will be occurring in the carbonator, reducing the available heat to recover from the carbonation reaction (of course, the stream could also go into the calciner). Assuming an atmospheric pressure hydrator, the maximum temperature of operation – i.e., at 101 kPa steam pressure – would be ≈793 K (calculated by use of thermodynamic data from NASA Glenn [8]). In practice, the temperature would be lower than this (i) because the steam pressure is likely to be lower and

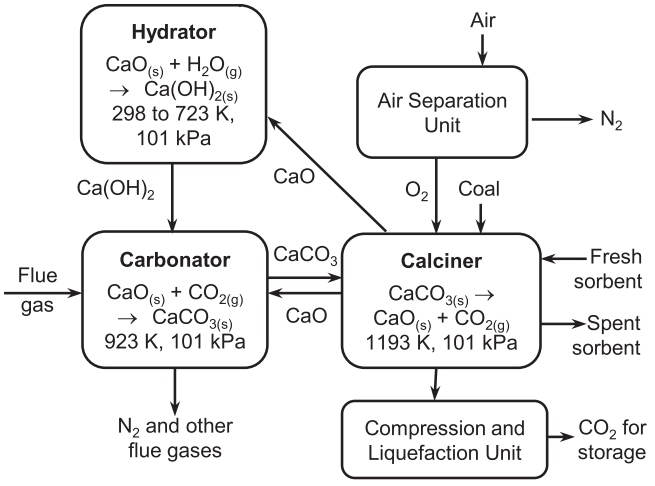

Fig. 1. Simplified schematic of a calcium looping process for post-combustion CO_2 capture with a reactivator/hydrator.

(ii) in order to increase the difference between the equilibrium concentration and steam pressure to enhance the driving force of the hydration reaction. A fraction of the solids from the calciner are sent to the hydrator, rather than back to the carbonator, whereupon CaO reacts with steam exothermically to form calcium hydroxide (Rn. (2)). The hydrated solids are then returned to the carbonator, whereupon they exhibit an increased reactivity towards CO_2 [9–11]. The solids are taken from the calciner to ensure as high a hydration conversion as possible; $CaCO_3$ formed in carbonation can form a shell across which limited diffusion takes place [11,12]. The solids are then returned to the carbonator in order to achieve higher conversions to $CaCO_3$ and reduced attrition than if returned to the calciner [13,14]. Arias et al. [15] have shown that, even with hydration conversions as low as 60%, the carrying capacity of sorbents in the system could be significantly enhanced, increasing capture efficiency and reducing the necessary amount of material in the system. This enhancement will involve a trade-off with the increased costs of generating steam and would be improved further by increasing the hydration conversion [16]. It should be noted that, while most researchers consider periodic hydration of sorbent, researchers at Ohio State University have developed a process whereby sorbent is hydrated between every calcination and carbonation [17]. The mechanism of enhancement is not clear, but work on the analogous reactivation process for sulphur capture from FBCs suggests that H_2O molecules penetrate the product layer more readily than CO_2 and result in the opening up of pores and new surface area of the sorbent [18]. Particles have also been shown to be prone to fracture upon hydration [10,19,20], which would also increase reactive porosity.

However, while there have been many general papers on the effects of using hydrated sorbent for CO_2/SO_2 capture, few have investigated the kinetics of the gas–solid reaction of H_2O with CaO. Maciel-Camacho et al. [21] investigated the hydration kinetics of lime pellets at low temperatures (less than 373 K) and low partial pressures of water vapour (1.2–3.6 kPa). Shiying Lin and colleagues [22–24] have published several papers on high-temperature and high-pressure hydration of various calcined limestones in a pressurised thermogravimetric analyser in relation to the HyPr-RING process. HyPr-RING is a pressurised gasification process with in situ CO_2 capture, which occurs under pressures that also allow in situ hydration. They investigated hydration rates

at 773–1023 K and pressures of 0.67–3.8 MPa. Serris et al. [25] have investigated the hydration of calcined limestones temperature range of 343–693 K (though mostly <423 K) with hydration pressures of between 0.5 and 16 kPa. Serris et al. [25] report an anti-Arrhenius effect (i.e., rates decrease with increasing temperature), which is contrary to findings by Maciel-Camacho et al. [21]. All researchers reported an increase in hydration kinetics with increasing partial pressure of steam/water [21–25], and, where studied, low activation energies (19.9 [21], 8.4 [23] and 11–20.3 [24] kJ/mol) and reduced kinetics for more highly sintered particles/pellets [21,25]. Criado et al. [26] and Schaube et al. [27] have recently investigated the kinetics of hydration with relation to energy storage applications. Criado et al. [26] demonstrated that a shrinking core model, with assumed equimolar counterdiffusion, could be used to effectively model the steam hydration of lime by investigating the kinetics for a variety of particle sizes.

This paper is a follow up to previous work [28], which showed that the hydration temperature and prior cycling conditions have a significant influence on the conversion to calcium hydroxide. Here, the experiments have been modified in order to further investigate the kinetics of the gas–solid reaction of H_2O with calcined limestone at elevated hydration temperatures (473–673 K). This paper develops work previously performed by Maciel-Camacho et al. [21] and Criado et al. [26], who have shown that a shrinking core model with equimolar counterdiffusion can be used to effectively model the hydration reaction. A shrinking core model with a non-equimolar scenario – as is the case for the hydration reaction – has been developed and applied to a wide range of experimental data for different hydration temperatures and CaO of different porosities. This paper does not comment on the reactivity of the hydrated sorbents towards CO_2; however, the assumption is that subsequent carbonation conversion will increase with increasing hydration conversion (as shown in, e.g. Blamey et al. [28]). A shrinking core model is then applied to the experimental data.

2. Experimental

Experiments were carried out in a similar manner to experiments described elsewhere [28]; the primary difference is the mass of calcined material for kinetic experiments, which has been reduced here in order to reduce effects of mass transfer through the sample. Samples of Havelock limestone (purity 96.3% $CaCO_3$, full elemental analysis published elsewhere [19]) were subjected to a number of cycles (N) of carbonation and calcination in a small bench-scale fluidised bed reactor (development described elsewhere [19]) before being removed following calcination. Subsequently, aliquots of these samples were taken and subjected to hydration in a thermogravimetric analyser (TGA) at various hydration temperatures for kinetics experiments. The maximum value investigated for N, the cycle number before hydration, was 13. This corresponds to a carbonation conversion of available CaO sites of 14% (or 10 g CO_2/g calcined sorbent) [19]. Therefore, a system whereby reactivation of sorbent is done after a relatively small number of cycles is investigated – as discussed by Martinez et al. [16] – rather than deep reactivation of highly unreactive sorbent after larger numbers of cycles (e.g., sorbent of reactivity of 6% after 50 cycles).

2.1. Cycling experiments

The cycles of carbonation and calcination in the fluidised bed reactor [19] were performed using 4.3 g of Havelock limestone (500–710 μm) in a bed of 13.0 g sand (355–425 μm). Calcination was carried out at 1173 K for 900 s and carbonation was carried out at 973 K for 900 s. Both calcination and carbonation were carried out at 101 kPa under a 15% (v/v) CO_2, balance N_2, atmosphere with a cold (293 K) flow-rate of 47.5 cm^3/s, which corresponded to $U/U_{mf} \approx 7$ at 973 K. Samples were cycled for 0 cycles (i.e., one calcination, with no carbonation), 2 cycles (1 calcination with 2 cycles of carbonation and calcination), 6 cycles or 13 cycles, before being removed from the fluidised bed following the final calcination and placed in a desiccator. Then, the samples were sieved to obtain sorbent particles >500 μm – i.e., to separate the limestone from the sand – and stored in a vial within a desiccated jar prior to steam hydration in the TGA.

2.2. Hydration experiments

Hydration was carried out in a TGA (Perkin Elmer TGA 7) on 4.5 ± 0.5 mg aliquots of sorbent particles; this represents a well-dispersed monolayer of particles. Hydration was carried out at average temperatures of 473, 573 and 673 K. In each case, samples had unavoidably hydrated slightly during transfer/separation (less than 13%), and, therefore, were first heated to 673 K at 0.83 K/s under N_2, cold flow-rate 10 cm^3/s, to dehydrate before the temperature set-point was changed to the hydration temperature. The samples were <1% carbonated; therefore, no prior decarbonation was deemed necessary. The furnace was turned off and the sample cooled prior to stabilisation at the desired temperature for 300 s. Cooling and stabilisation took 300 s at 673 K, 1080 s at 573 K, and 1620 s at 473 K. Then, reaction gas, with an equivalent total cold (293 K, 101 kPa) flow-rate of 100 cm^3/s was injected to the system. The steam was generated using a syringe pump and a steam generation system and was preheated before injection. The steam system was preheated to 423 K and entered the TGA at atmospheric pressure. Hydration was performed for a total of 900 s. Note that the partial pressures of steam over $Ca(OH)_2$ (see Rn. (2)) at equilibrium at 473, 573 and 673 K are 0.002, 0.26 and 6.8 kPa [8,19]. The reaction gas was 10% steam, balance N_2, in the case of 473 and 573 K, and 20% steam, balance N_2, in the case of 673 K; this was to keep $X_B - X_E$ approximately constant at near 10%.

3. Results

3.1. Physical properties of cycled sorbent

The cycled sorbent (i.e., the sorbent prior to hydration) was subjected to nitrogen adsorption (Micromeritics Tristar 3000 N_2 Sorption Analyser) and mercury porosimetry (Micromeritics Autopore IV) analyses to establish the BET surface area, the BJH porosity associated with small pores, the skeletal density and total porosity (see Table 1). Data show that the BET surface area and the porosity associated with small pores ($\lesssim$1 μm) decreased markedly upon cycling; the BJH porosity associated with small pores decreased more gradually than the surface area. The approximate total porosity (5 nm to 360 μm) also decreased and the envelope density (the density including pores) increased markedly (an increase of ≈40%).

Table 1
Physical properties of cycled limestone, taken from nitrogen adsorption and mercury porosimetry analysis.

Number of cycles	BET surface area [m^2/g]	BJH porosity $\lesssim$1 μm [%]	MP porosity ≈ 5 nm–360 μm [%]	MP envelope density [g/cm^3]
0	16.17	27.4	68.5	1.01
2	8.77	22.9	59.7	1.29
6	5.15	15.3	56.6	1.39
13	2.88	7.9	55.3	1.43

The surface area and porosities of the samples shown are for the calcined sorbent *prior* to hydration.

3.2. Hydration behaviour as a function of cycle number

Fig. 4 shows conversion to $Ca(OH)_2$ of available CaO (mol/mol) as a function of time for all samples tested (0, 2, 6 and 13 cycles) at 473 K, 573 K and 673 K. Note that 100% conversion corresponds to 0.30 g H_2O per g calcined sorbent. Data obtained at both temperatures show that it became progressively more difficult to hydrate the sample as the number of cycles before hydration increased. At 473 K, the samples hydrated after 0 and 2 cycles were hydrated to 90% within ≈450 s; however, the sample hydrated after 13 cycles only achieved hydration of 30% after 900 s. At 673 K, the sample hydrated after 0 cycles hydrated very quickly; however, the samples hydrated after 2, 6 and 13 cycles appeared to reach a maximum/limiting conversion after which the rate of reaction became very slow and the overall conversion to $Ca(OH)_2$ was low after 900 s. This is most likely from pore blockage resulting in very slow gas diffusion through pores or solid–state diffusion; though this was less clear than observed in previous work [28] with larger sample sizes (4.5 vs 18 mg). This state is reached more rapidly for the samples cycled to greater extents, because of their reduced porosity associated with small pores (see BJH porosity of Table 1), which are more prone to blocking upon formation of $Ca(OH)_2$, which has a higher specific volume per mole of CaO present. The lower overall porosity will have an effect also – see mercury porosimetry porosity data of Table 1.

3.3. Hydration conversion at 900 s and maximum observed rate

Fig. 2 shows the conversion to $Ca(OH)_2$ of available CaO sites at 900 s and maximum observed rate. The maximum conversion of CaO to $Ca(OH)_2$ at 900 s tended to decrease with increasing cycle number and increasing hydration temperature. In addition, the rate decreased with increasing cycle number and increasing hydration temperature. As such, increasing hydration temperature resulted in a reduced rate and a reduced conversion to $Ca(OH)_2$ after 900 s. The reduced conversion support the blocking effect and the anti-Arrhenius behaviour observed by Serris et al. [25] and explored for similar experiments elsewhere [28].

4. Shrinking Core Model

A Shrinking Core Model (SCM) has been developed to describe the kinetics of hydration of CaO. It considers non-equimolar counter-diffusion, as is the case in the hydration reaction. It should be noted that the model developed is for a particle of constant diameter, whereas particles have been shown to expand upon hydration [19]; this assumption is good as a first approximation, but is worthy of further study.

4.1. Model assumptions

The assumptions of the SCM are:

- The hydration of calcium oxide (Rn. (2)) occurs at the interface of a pure, porous, unreacted CaO core and a pure, porous, $Ca(OH)_2$ product layer (see Fig. 3);
- The external particle size remains constant during reaction;
- Diffusion through the bulk phase to the particle surface follows Chapman–Enskog theory [29];
- Particles are treated as isolated spheres;
- Mass transfer through a product layer of uniform porosity and pore size is modelled considering bulk diffusivity and Knudsen diffusivity as resistances in series;
- The reaction kinetics at the surface of the core are first order;
- The system remains isothermal upon reaction.

4.2. Model development

The full model derivation is outlined in Supplementary information.

4.2.1. Bulk diffusivity and mass transfer coefficients

The gas-phase diffusivity was calculated from Chapman–Enskog theory (see Table 2) [29]. The collision diameter of the gas mixture and the collision integral were calculated using a equations and data provided by Cussler [29]. The Sherwood Number for this work has been estimated using a correlation from Perry and Green [30], which is dependent on the Reynolds and Schmidt Numbers. Fluid viscosities and densities were obtained from the NIST Chemistry Webbook [31] and the fluid velocity was calculated for the temperatures of interest using a cold (293 K) inlet flow-rate

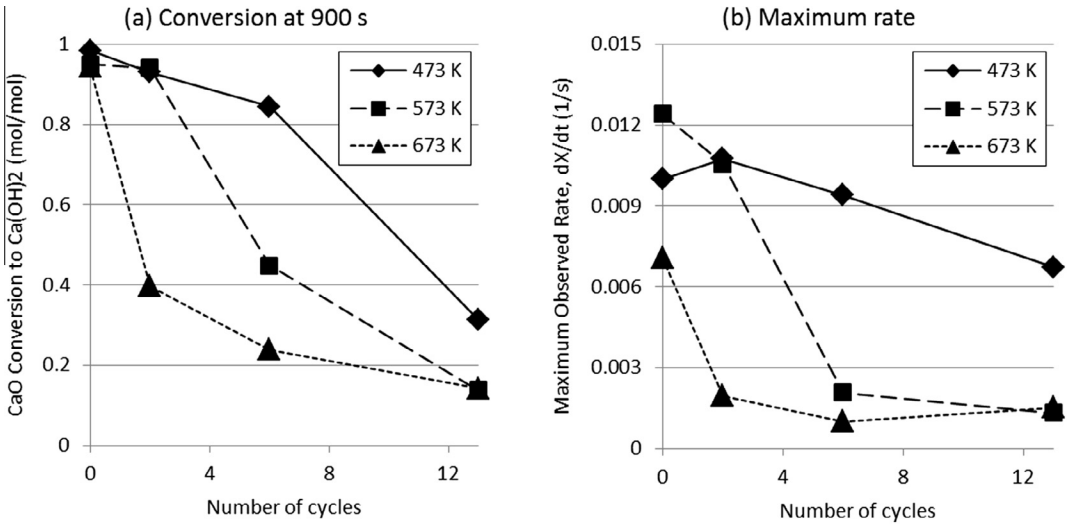

Fig. 2. (a) Hydration conversion of CaO to $Ca(OH)_2$ at 900 s and (b) maximum observed rates of reaction (the differential of the conversion against time) as a function of cycle number.

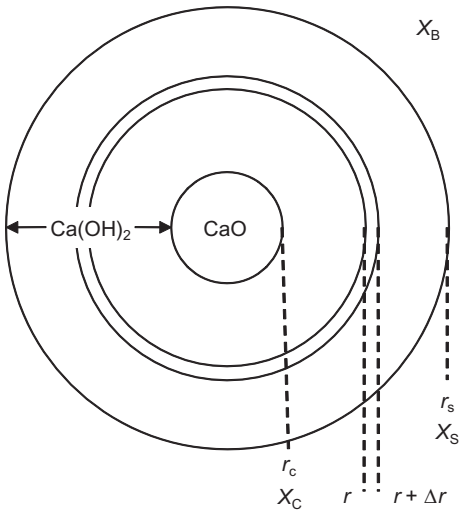

Fig. 3. Shrinking core model; where r is the radius of the particle and X is the mole fraction of steam with subscripts 'c/C', 's/S' and 'B' denoting at the core, at the (external) surface and in the bulk respectively.

Table 2
Calculated values of gas phase diffusivities and mass transfer coefficients at the temperatures of investigation.

Temperature of hydration [K]	473	573	673
Gas phase diffusivity [m^2/s]	5.15×10^{-5}	7.30×10^{-5}	9.73×10^{-5}
Mass transfer coefficient [m/s]	0.154	0.201	0.249

of 100 cm^3/s and an internal diameter of the TGA furnace of 17 mm. As a result, an estimate of the mass transfer coefficient (k_g) was calculated (see Table 2) for the temperatures of interest from the Sherwood Number, gas-phase diffusivity and the particle diameter.

The mass transfer coefficient can be used to calculate the flux of H_2O at the surface of the particle (W_{H_2O,r_s}), with knowledge of the molar bulk and surface concentrations of H_2O (C_B and C_S respectively), using Eq. (1). Assuming a perfect gas, the mole fractions of H_2O can be calculated from $C_x = CX_x$.

$$W_{H_2O,r_s} = -k_g C(X_B - X_S) \quad (1)$$

4.2.2. Intra-particle diffusivity

The mechanism of diffusion through the particle has to be established, in order to calculate the intra-particle diffusivity. To establish whether Knudsen diffusion contributes, the mean free path of molecules has to be compared to the average pore diameter; Knudsen diffusion occurs when molecules collide with pore walls more frequently than with other molecules. The mean free path was calculated, using as 208, 252 and 296 nm for 473, 573 and 673 K respectively. The pore size distribution of the Ca(OH)$_2$ product layer through which the steam diffuses to react with the CaO was not directly measured. Therefore, it was calculated indirectly, using data obtained for porosity (obtained from mercury porosimetry measurements, <360 μm) and average pore diameter (as obtained from nitrogen adsorption studies) for the cycled CaO. First, the porosity of Ca(OH)$_2$ was calculated from a mass balance of CaO and Ca(OH)$_2$, assuming no change in particle/layer size (see Eq. (2)). Then, the average pore size was calculated, assuming a constant pore length (see Eq. (3)), i.e., constant growth along the length of the pore. Experimental data for CaO and calculated data for Ca(OH)$_2$ are presented in Table 3.

$$\varepsilon_{Ca(OH)_2} = 1 - \frac{\rho_{CaO} M_{Ca(OH)_2} (1 - \varepsilon_{CaO})}{\rho_{Ca(OH)_2} M_{CaO}} \quad (2)$$

$$d_{pore,Ca(OH)_2} = \frac{d_{pore,CaO} \varepsilon_{Ca(OH)_2}}{\varepsilon_{CaO}} \quad (3)$$

The pore diameter (7–14 nm) is therefore smaller than the mean free path length (λ, 210–300 nm). The Knudsen numbers (λ/d_{pore}) are between 15 and 45 – depending on extent of cycling and temperature of hydration, which are within the range in where Knudsen diffusion is expected. The Knudsen diffusivity (D_K) was calculated according to Eq. (4) (see Table 4), using the molar mass of H_2O [29]. Then, the effective diffusivity (D_e) through the pores was derived according to Eq. (5) using the conventional expression for resistances in series [32] combined with a term to account for porosity and pore tortuosity [29] (see Table 4). The pore tortuosity (τ_{pore}), which is a factor to account for the non-linear nature of pores, was taken as 3; this is a typical value suggested, in absence of experimental data, by Cussler [29].

$$D_K = \frac{1}{3} d_{pore} \left(\frac{2RT}{\pi M_{H_2O}} \right)^{1/2} \quad (4)$$

$$D_e = \frac{\varepsilon_{Ca(OH)_2}}{\tau_{pore}} \left(\frac{1}{D_g} + \frac{1}{D_K} \right)^{-1} \quad (5)$$

4.2.3. Mass transfer through the product layer

The constitutive equation (or Fick's law) for a constant molar concentration can be used to derive Eq. (6) for the hydration of lime, where there is one diffusing species, H_2O, and no counter-diffusing species.

$$W_{H_2O,r} = \frac{-CD_e}{(1 - X_{H_2O,r})} \frac{dX_{H_2O,r}}{dr} \quad (6)$$

A mass balance on the flux of H_2O (W_{H_2O}) between r and Δr in the product layer, as well as the consideration of two boundary conditions, results in the derivation of Eq. (7), the equation for molar flux through the product layer; at the first boundary condition (BC1) $r = r_S$ and $X_{H_2O,r} = X_S$, and at the second (BC2) $r = r_C$ and $X_{H_2O,r} = X_C$.

$$W_{H_2O,r} = \frac{-CD_e \ln \left[\frac{(1-X_S)}{(1-X_C)} \right]}{r^2 \left(\frac{1}{r_S} - \frac{1}{r_C} \right)} \quad (7)$$

4.2.4. Mass balance on Ca(OH)$_2$ formation during reaction

A balance on the number of moles of CaO at time t has been performed. Noting that (i) the rate of production of Ca(OH)$_2$ is the negative rate of production of CaO and (ii) the rate of production of Ca(OH)$_2$ is also the negative rate of production of H_2O, the rate of production of Ca(OH)$_2$ can be calulated and the rate of change of the core radius can be derived. A constant external diameter of particles has been assumed; therefore, the radius at the core can be related to the conversion to Ca(OH)$_2$ ($X_{Ca(OH)_2}$) within the particles. This gives a relationship between experimentally derived rates of

Table 3
Experimental data for CaO and calculated data for Ca(OH)$_2$.

Cycle number	CaO porosity	CaO average pore diameter [nm]	Ca(OH)$_2$ porosity	Ca(OH)$_2$ average pore diameter [nm]
0	0.685	25.6	0.372	13.9
2	0.597	34.2	0.196	11.2
6	0.566	36.0	0.134	8.6
13	0.553	34.0	0.109	6.7

Table 4
Calculated Knudsen and effective diffusivity for hydration temperatures and cycling extents investigated.

Cycle number	Knudsen diffusivity [m^2/s]			Effective diffusivity [m^2/s]		
	At 473 K	At 573 K	At 673 K	At 473 K	At 573 K	At 673 K
0	3.45×10^{-6}	3.80×10^{-6}	4.11×10^{-6}	4.00×10^{-7}	4.47×10^{-7}	4.89×10^{-7}
2	2.79×10^{-6}	3.08×10^{-6}	3.33×10^{-6}	1.73×10^{-7}	1.93×10^{-7}	2.11×10^{-7}
6	2.13×10^{-6}	2.34×10^{-6}	2.54×10^{-6}	9.16×10^{-8}	1.02×10^{-7}	1.11×10^{-7}
13	1.66×10^{-6}	1.83×10^{-6}	1.98×10^{-6}	5.84×10^{-8}	6.48×10^{-8}	7.05×10^{-8}

reaction and the flux of H_2O at the interface of the core and the product layer. Similar derivations are given in, e.g., Fogler [33].

$$\frac{dX_{Ca(OH)_2}}{dt} = \frac{-3}{r_s}(1 - X_{Ca(OH)_2})^{2/3} \frac{M_{CaO} W_{H_2O,r_c}}{\rho_{CaO}(1 - \varepsilon_{CaO})} \quad (8)$$

4.2.5. First order kinetics of reaction

First order reaction kinetics is assumed and therefore the rate of formation of $Ca(OH)_2$ is given in Eq. (9), where k_A is the first order rate constant per unit surface area, S_V is the BET surface area per unit volume (using data presented in Table 1, expressed in m^2/m^3, calculated from $S_V = S_{BET}\rho_{CaO}(1 - \varepsilon_{CaO})$) and X_C and X_E are the mole fraction of H_2O at the core and the mole fraction associated with the equilibrium partial pressure of H_2O over $Ca(OH)_2$ at the temperature of hydration respectively. $(X_C - X_E)$ is chosen as the effective mole fraction of H_2O driving the reaction; note that the reaction will cease if $X_C = X_E$.

$$\frac{d(n_{Ca(OH)_2})}{dt} = \frac{4\pi r_c^3 S_V}{3} k_A C (X_C - X_E) \quad (9)$$

The molar rate of reaction of $Ca(OH)_2$ is related to the flux of H_2O at the interface of the core and the product layer using Eq. (10); it therefore follows that the flux of H_2O at the interface can be presented by Eq. (11).

$$W_{H_2O,r_c} = \frac{-1}{4\pi r_c^2} \frac{d(n_{Ca(OH)_2})}{dt} \quad (10)$$

$$W_{H_2O,r_c} = \frac{-r_c S_V}{3} k_A C (X_C - X_E) \quad (11)$$

4.2.6. Application of the Shrinking Core Model

To recap, the key equations are: (i) Eq. (1) for mass transfer of H_2O to the particle surface; (ii) Eq. (7) for mass transfer of H_2O through the product layer; (iii) Eq. (11) for mass transfer of H_2O to form $Ca(OH)_2$ by reaction; and (iv) Eq. (8) relating mass transfer of H_2O at the interface of the core and the product layer to experimental data.

A solution for k_A was found for each set of experimental conditions separately (i.e., for each hydration temperature and number of cycles before hydration). Initially, 41 data points were taken from each experiment at *equal conversion increments* for conversions to $Ca(OH)_2$ of between 0.05 and either 0.95, if full conversion was achieved, or the final conversion at t = 1080 s. Subsequently, X_S and X_C were calculated for all data points, using values of $dX_{Ca(OH)_2}/dt$ and $X_{Ca(OH)_2}$ determined experimentally. X_S and X_C could not be calculated analytically and, therefore, were established numerically using a script written in Matlab. Then, k_A was calculated for each experiment from Eq. (11) by a least squares method across all data points using a script written in Matlab. In this way, a value of k_A was established for each set of experimental conditions. The values of k_A obtained were then used to obtain projected idealised model results for X_S, X_C and $X_{Ca(OH)_2}$ as a function of time.

5. Shrinking Core Model results and discussion

Data obtained for k_A are given in Table 5, and plots of projected conversions as a function of time from the SCM are given in comparison to experimental data in Fig. 4.

From inspection of Fig. 4, model data is observed to track experimental data successfully and the more major deviations can be described as:

- The model tends to over-predict the rate at low conversions for the samples only calcined once (i.e., 0 cycles);
- The model tends to over-predict the rate at higher conversions for the more heavily cycled samples at higher hydration temperatures.

The reason for the over-prediction at lower conversions for the sample calcined once is likely to be mass transfer through to the centre and base of the pan. This would result in lower concentrations at the surfaces of particles in these positions and consequential lower rates of reaction observed experimentally. This would be especially pronounced when time is close to zero and for the experiments where the rate of reaction is faster. This explains why the effect is most pronounced for the samples calcined only once, but it is also observed to a lesser extent for most other experiments.

The reason for the over-prediction at higher conversions for the samples at (i) higher cycling extents and (ii) higher temperatures is likely to result from pore closure as well as the method of solution of the model. Pore closure owing to surface sintering is more likely in these cases, because (i) the samples are less porous at higher cycling extents and, even if the larger pores do not close, smaller reactive pores will be prone to closure upon formation of the less

Table 5
Rate constants per unit area for the hydration of CaO (see Eq. (11)) for all hydration temperatures and cycling extents tested.

Number of cycles	k_A – rate constant per unit area [m/s]		
	At 473 K	At 573 K	At 673 K
0	6.55×10^{-7}	5.60×10^{-7}	5.52×10^{-7}
2	6.61×10^{-7}	6.63×10^{-7}	1.13×10^{-7}
6	3.73×10^{-7}	1.56×10^{-7}	9.33×10^{-8}
13	1.23×10^{-7}	5.80×10^{-8}	7.08×10^{-8}

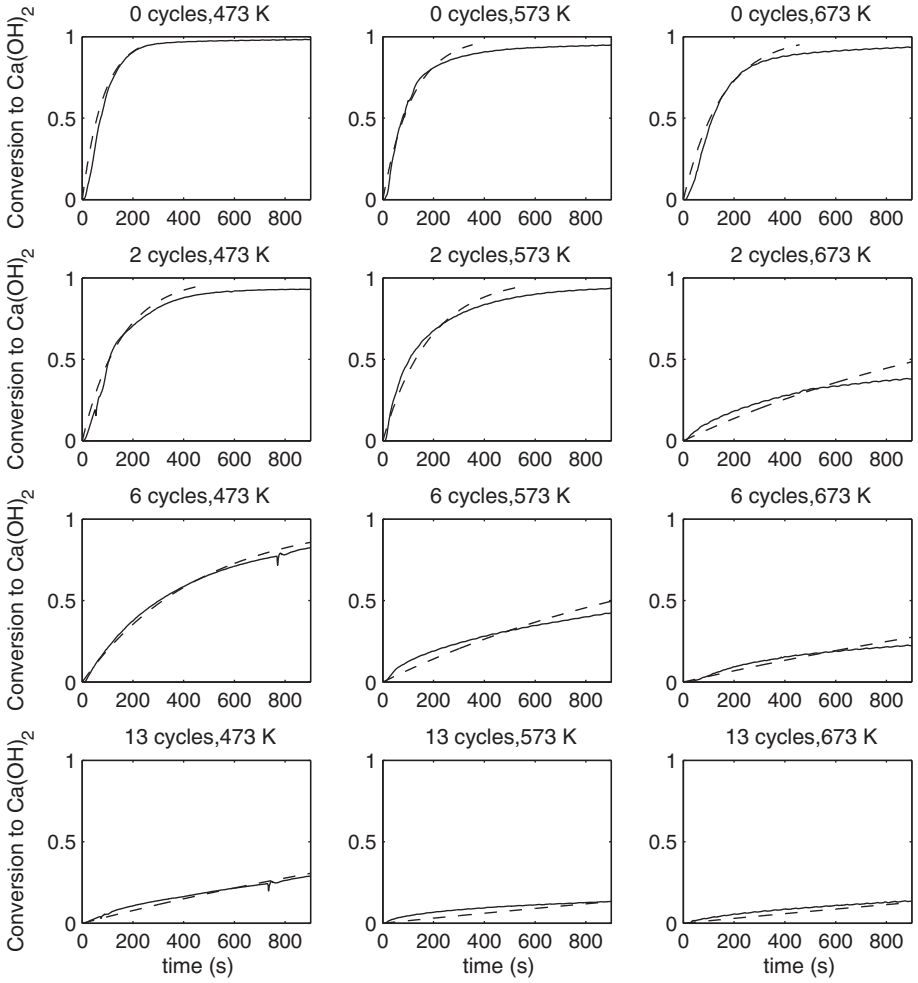

Fig. 4. Plots of projected conversion to $Ca(OH)_2$ as a function of time as calculated by the SCM (dashed lines) against experimental data (solid lines); note that all plots in the same y position have the same cycle number (0, 2, 6 or 13) and all in the same x position have the same hydration temperature (473, 573 or 673 K); *x* axis limits kept constant for experiments of the same cycle number.

dense $Ca(OH)_2$ from CaO, and (ii) sintering of $Ca(OH)_2$ is accelerated at higher temperatures. Pore closure would result in a necessary change of mechanism from gaseous diffusion of H_2O molecules to an ^{-}OH solid-state diffusion mechanism. It should be noted that, if porosity is to be closed in the model, lower values of initial porosity should be used (i.e., less than 180 μm rather than 360 μm – or only those associated with small pores, e.g., <1 μm). Another reason for the significant overshoot of conversion at higher times is that the model was developed with data chosen at incremental steps of conversion. As a result, there are fewer data points from higher time periods (because the rate of change in conversion is much lower). This results in an increased weighting to the kinetic data obtained at lower times. If time had been used as the increment the conversion after ≈600 s would be much more accurate; however, the initial rate would then be considerably underestimated. There may also be further errors in the geometrical assumptions of the model introduced by (i) the non-spherical nature of particles and (ii) the fact that large cracks and large pores will be present in the limestone.

Table 5 shows that no significant trends for k_A are observed, except that it decreases with increasing number of cycles and there is a general tendency to decrease with increasing temperature. The value of k_A should be constant for all cycle numbers at the same hydration temperature, because this is the intrinsic rate of reaction of CaO per available surface area. The fact that it is not consistent suggests a breakdown of the model at higher cycle numbers. One potential explanation for the deviation at higher cycle numbers is the shift to a reaction based on solid state diffusion, which is more important in systems where pore closure is observed. Accurate modelling of this process would require additional terms in the shrinking core model. A decreasing value of k_A with increasing temperature would be consistent with anti-Arrhenius behaviour observed by Serris et al. [25].

6. Concluding remarks

A study has been undertaken in a TGA that investigates the kinetics and maximum conversion to $Ca(OH)_2$ of cycled CaO upon reaction with steam at three temperatures between 473 and 673 K. It has been shown that:

- Samples cycled minimally (1 calcination or 2 cycles) readily hydrate to completion across all temperatures;
- Rate of hydration decreases with increasing cycle number, because of the lower reactive surface areas;
- Maximum hydration extent over the 900 s of hydration decreased with increasing cycle number and increasing hydration temperature;
- A shrinking core model incorporating non-equimolar counter-diffusion has been developed and fitted to data, which fits the data well

- However, inconsistencies of the value of k_A at higher cycle numbers suggest a break-down of the shrinking core model, likely due to pore closure and mechanism change from gaseous diffusion to solid-state diffusion.

These findings have important ramifications for the use of hydration as a reactivation strategy. Ideally, higher hydration temperatures would be used to reclaim higher grade heat from the exothermic hydration reaction; this might have to be done at the expense of hydration conversion, which decreases at higher temperatures. In addition, there is likely to be more benefit from reactivating extensively cycled/sintered sorbent; however, the most highly cycled sample tested here showed the lowest hydration conversion and is therefore likely to show the lowest reactivity upon further carbonation (hydration extent and subsequent carbonation extent have been linked elsewhere [28]). It should be noted that this can correspond to a greater increase in comparative carbonation conversion than samples achieving full conversion after fewer cycles, which already showed high carbonation conversions.

Data Statement

TGA Data for conversion to $Ca(OH)_2$ from CaO as a function of time is available as Supplementary Data. Additional data queries should be sent to the corresponding author.

Acknowledgements

The authors wish to thank the Engineering and Physical Sciences Research Council (UK) for funding the studentship of John Blamey. Follow up work was funded in part by Carbon Management Canada and the Engineering and Physical Sciences Research Council, under the G8-2012 Research Councils Initiative on Multilateral Research Funding (EP/K021710/1) and the UK Carbon Capture and Storage Research Centre (EP/K000446/1).

Appendix A. Supplementary data

Supplementary data associated with this article can be found, in the online version, at http://dx.doi.org/10.1016/j.cej.2016.01.086.

References

[1] B. Arias, M.E. Diego, J.C. Abanades, M. Lorenzo, L. Diaz, D. Martínez, J. Alvarez, A. Sánchez-Biezma, Demonstration of steady state CO_2 capture in a 1.7 MWth calcium looping pilot, Int. J. Greenhouse Gas Control 18 (2013) 237–245.
[2] J. Kremer, A. Galloy, J. Ströhle, B. Epple, Continuous CO_2 capture in a 1-MWth carbonate looping pilot plant, Chem. Eng. Technol. 36 (9) (2013) 1518–1524.
[3] M. Alonso, M.E. Diego, C. Pérez, J.R. Chamberlain, J.C. Abanades, Biomass combustion with in situ CO_2 capture by CaO in a 300 kWth circulating fluidized bed facility, Int. J. Greenhouse Gas Control 29 (2014) 142–152.
[4] H. Dieter, A.R. Bidwe, G. Varela-Duelli, A. Charitos, C. Hawthorne, G. Scheffknecht, Development of the calcium looping CO_2 capture technology from lab to pilot scale at IFK, University of Stuttgart, Fuel 127 (2014) 23–37.
[5] T. Shimizu, T. Hirama, H. Hosoda, K. Kitano, M. Inagaki, K. Tejima, A twin fluid-bed reactor for removal of CO_2 from combustion processes, Chem. Eng. Res. Des. 77 (1) (1999) 62–68.
[6] J. Blamey, E.J. Anthony, J. Wang, P.S. Fennell, The calcium looping cycle for large-scale CO_2 capture, Prog. Energy Combust. Sci. 36 (2) (2010) 260–279.
[7] W. Liu, H. An, C. Qin, J. Yin, G. Wang, B. Feng, M. Xu, Performance enhancement of calcium oxide sorbents for cyclic CO_2 capture—a review, Energy Fuels 26 (5) (2012) 2751–2767.
[8] B.J. McBride, M.J. Zehe, S. Gordon, NASA Glenn Coefficients for Calculating Thermodynamic Properties of Individual Species, National Aeronautics and Space Administration, Cleveland, Ohio, US, 2002.
[9] P.S. Fennell, J.F. Davidson, J.S. Dennis, A.N. Hayhurst, Regeneration of sintered limestone sorbents for the sequestration of CO_2 from combustion and other systems, J. Energy Inst. 80 (2) (2007) 116–119.
[10] R.W. Hughes, D. Lu, E.J. Anthony, Y.H. Wu, Improved long-term conversion of limestone-derived sorbents for in situ capture of CO_2 in a fluidized bed combustor, Ind. Eng. Chem. Res. 43 (18) (2004) 5529–5539.
[11] V. Manovic, E.J. Anthony, Steam reactivation of spent CaO-based sorbent for multiple CO_2 capture cycles, Environ. Sci. Technol. 41 (4) (2007) 1420–1425.
[12] P. Sun, J.R. Grace, C.J. Lim, E.J. Anthony, Investigation of attempts to improve cyclic CO_2 capture by sorbent hydration and modification, Ind. Eng. Chem. Res. 47 (6) (2008) 2024–2032.
[13] V. Materic, S. Edwards, S.I. Smedley, R. Holt, $Ca(OH)_2$ superheating as a low-attrition steam reactivation method for CaO in calcium looping applications, Ind. Eng. Chem. Res. 49 (24) (2010) 12429–12434.
[14] V. Materic, S.I. Smedley, High temperature carbonation of $Ca(OH)_2$, Ind. Eng. Chem. Res. 50 (10) (2011) 5927–5932.
[15] B. Arias, G.S. Grasa, J.C. Abanades, Effect of sorbent hydration on the average activity of CaO in a Ca-looping system, Chem. Eng. J. 163 (3) (2010) 324–330.
[16] I. Martinez, G. Grasa, R. Murillo, B. Arias, J.C. Abanades, Evaluation of CO_2 carrying capacity of reactivated CaO by hydration, Energy Fuels 25 (3) (2011) 1294–1301.
[17] W. Wang, S. Ramkumar, D. Wong, L.S. Fan, Simulations and process analysis of the carbonation–calcination reaction process with intermediate hydration, Fuel 92 (1) (2012) 94–106.
[18] E.J. Anthony, E.M. Bulewicz, L. Jia, Reactivation of limestone sorbents in FBC for SO_2 capture, Prog. Energy Combust. Sci. 33 (2) (2007) 171–210.
[19] J. Blamey, N.P.M. Paterson, D.R. Dugwell, P.S. Fennell, Mechanism of particle breakage during reactivation of CaO-based sorbents for CO_2 capture, Energy Fuels 24 (2010) 4605–4616.
[20] V. Materic, C. Sheppard, S.I. Smedley, Effect of repeated steam hydration reactivation on CaO-based sorbents for CO_2 capture, Environ. Sci. Technol. 44 (24) (2010) 9496–9501.
[21] A. Maciel-Camacho, H. Rodriguez Hernandez, A.W.D. Hills, R.D. Morales, Hydration kinetics of lime, ISIJ Int. 37 (5) (1997) 468–476.
[22] S. Lin, Y. Wang, Y. Suzuki, High-temperature CaO hydration/$Ca(OH)_2$ decomposition over a multitude of cycles, Energy Fuels 23 (2009) 2855–2861.
[23] S.Y. Lin, M. Harada, Y. Suzuki, H. Hatano, CaO hydration rate at high temperature (similar to 1023 K), Energy Fuels 20 (3) (2006) 903–908.
[24] Y. Wang, S.Y. Lin, Y. Suzuki, Effect of CaO content on hydration rates of Ca-based sorbents at high temperature, Fuel Process. Technol. 89 (2) (2008) 220–226.
[25] E. Serris, L. Favergeon, M. Pijolat, M. Soustelle, P. Nortier, R.S. Gartner, T. Chopin, Z. Habib, Study of the hydration of CaO powder by gas–solid reaction, Cem. Concr. Res. 41 (10) (2011) 1078–1084.
[26] Y.A. Criado, M. Alonso, J.C. Abanades, Kinetics of the CaO/$Ca(OH)_2$ hydration/dehydration reaction for thermochemical energy storage applications, Ind. Eng. Chem. Res. 53 (32) (2014) 12594–12601.
[27] F. Schaube, L. Koch, A. Wörner, H. Müller-Steinhagen, A thermodynamic and kinetic study of the de- and rehydration of $Ca(OH)_2$ at high H_2O partial pressures for thermo-chemical heat storage, Thermochim. Acta 538 (2012) 9–20.
[28] J. Blamey, V. Manovic, E.J. Anthony, D.R. Dugwell, P.S. Fennell, On steam hydration of CaO-based sorbent cycled for CO_2 capture, Fuel 150 (2015) 269–277.
[29] E.L. Cussler, Diffusion: Mass Transfer in Fluid Systems, 3rd ed., Cambridge University Press, 2009.
[30] R.H. Perry, D.W. Green, Perry's Chemical Engineers' Handbook, seventh ed., McGraw-Hill, New York, USA, 1997.
[31] E.W. Lemmon, M.O. McLinden, D.G. Friend, Thermophysical Properties of Fluid Systems in NIST Chemistry WebBook, NIST Standard Reference Number 69. Eds. P.J. Linstrom, W.G. Mallard. National Institute of Standards and Technology, Gaithersburg MD, USA. 2009; Available from: http://webbook.nist.gov.
[32] R.W. Missen, C.A. Mims, B.A. Saville, Introduction to Chemical Reaction Engineering and Kinetics, John Wiley & Sons, 1999.
[33] H.S. Fogler, Elements of Chemical Engineering, Pearson Education International, 2006.